LYAPUNOV STABILITY OF A TURBULENT BAROCLINIC JET IN A QUASIGEOSTROPHIC MODEL

Chris Snyder

*National Center for Atmospheric Research**

Boulder, CO

Thomas M. Hamill

NOAA-CIRES Climate Diagnostics Center

Boulder, CO

* The National Center for Atmospheric Research is sponsored by the National Science Foundation.

Corresponding author address: C. Snyder, NCAR, P.O. Box 3000, Boulder, CO 80307-3000; chriss@ucar.edu

ABSTRACT

Leading Lyapunov exponents and vectors are calculated for a turbulent baroclinic jet in a quasigeostrophic model with $O(10^5)$ degrees of freedom. The leading exponent is close to $0.4\,\mathrm{d}^{-1}$ and the unstable subspace has dimension between 30 and 40. The leading Lyapunov vectors exhibit a strong correlation of their potential vorticity (PV) with the PV gradients of the unperturbed flow. These perturbations do not, however, appear to be instabilities of smaller scale on the turbulent flow. Instead, they share the scales of the flow itself (at least if measured along PV contours) and often simply represent phase shifts or displacements of existing features in the flow. Singular vectors constrained to subspace of Lyapunov vectors are also calculated. Maximum amplification factors over two days are, on average, about 6, 7.5, and 9 (compared to the factor of two implied by the leading exponent) for subspaces of the leading 20, 35 and 60 Lyapunov vectors, respectively.

1. INTRODUCTION

Numerical models typically represent the governing equations for the atmosphere or ocean as a set of coupled, nonlinear ordinary differential equations. Given a (time dependent) solution from a certain initial condition, a natural question is then the stability of that solution to small perturbations of the initial condition. This is the problem of Lyapunov stability, which generalizes familiar linear stability analyses for steady flows and underlies characterizations of geophysical flows as chaotic. This note presents Lyapunov stability results for a damped and driven quasigeostrophic flow with broad similarity to the atmospheric midlatitude jet. Special emphasis will be given to the structure of the growing perturbations and their relation to the original, unperturbed flow.

Aside from its theoretical interest, Lyapunov stability provides information on the rate at which forecast errors grow and on the form that they will assume, at least in the case that the forecast model is reasonably accurate and the forecast errors are not too large. The results of Lyapunov stability also find application in areas such as ensemble forecasting (Toth and Kalnay 1997) and data assimilation (Swanson et al. 1998).

Excluding results from low-order models, little is known about the Lyapunov stability of atmospheric flows. Several studies have employed the same three-layer, quasigeostrophic, hemispheric model truncated at T21 (Vannitsem and Nicolis 1997; Swanson et al. 1998; Reynolds and Errico 1999). This notes complements and extends those previous studies by using a different quasigeostrophic model, with different geometry, different forcing and more degrees of freedom, and by characterizing the structure of the leading Lyapunov vectors and their relation to the unperturbed flow.

2. BACKGROUND

To fix ideas, let the unperturbed flow evolve according to

$$d\bar{\mathbf{x}}/dt = \mathbf{f}(\bar{\mathbf{x}}), \tag{1}$$

where $\bar{\mathbf{x}}(t)$ is the state of the flow in some discrete representation (such as spectral components or grid-point values). Perturbations $\mathbf{x}$ that are sufficiently small then satisfy $d\mathbf{x}/dt = A\mathbf{x}$ with A given by the Jacobian matrix of with respect to $\bar{\mathbf{x}}$; this relation may in turn be integrated over a time interval $[\tau, t]$ to yield

$$\mathbf{x}(t) = M(\bar{\mathbf{x}}, \tau, t)\mathbf{x}(\tau), \tag{2}$$

where M is the propagator or resolvent matrix and depends on the unperturbed solution and the time interval.

Lyapunov stability then concerns the behavior of solutions of (2) as $t - \tau \to \infty$. An excellent introduction to the theory as well as further references can be found in Legras and Vautard (1995). Here, we briefly review the points of importance to what will follow.

There are two key results. First, almost any initial perturbation will amplify exponentially when averaged over a sufficiently long interval; the rate of amplification defines the leading Lyapunov exponent, λ_1. This exponent is a property only of (1) and is independent of the specific unperturbed solution $\bar{\mathbf{x}}$ and of the choice of norm to measure the perturbation amplitude. Second, almost any perturbation initialized far in the past will converge at a future time t to a specific direction, given by the unit vector $\mathbf{w}_1(t)$. This is the leading Lyapunov vector (LV), which depends on t and implicitly on $\bar{\mathbf{x}}$.

More generally, there exists a sequence of exponents $\{\lambda_i\}$ and a corresponding set of orthonormal vectors $\{\mathbf{w}_i\}$ such that, given (almost) any set of N initial perturbations, the hypervolume defined by these perturbations grows on average exponentially at the rate $\sum_{i=1}^{N} \lambda_i$ and the subspace spanned by these perturbations converges after sufficient time to span $\{\mathbf{w}_1, \ldots, \mathbf{w}_N\}$. Because we require the LVs to be orthogonal, each $\mathbf{w}_i$ except the first depends on the choice of inner product.

Our numerical calculation of the exponents and the corresponding LVs $\{\mathbf{w}_i\}$ follows the standard method (see Legras and Vautard 1985). Specifically, N initial perturbations are integrated forward with the tangent linear model linearized about the unperturbed solution, with periodic orthonormalization using a modified Gram-Schmidt procedure and the total energy inner

product (as defined in Snyder et al, 2001). As the integration continues, the portion of the ith perturbation that is orthogonal to the subspace of the first $i-1$ perturbations converges to $\mathbf{w}_i$ and its average amplification converges to λ_i.

It is worth noting the analogy with traditional linear stability analyses of steady flows. In that case, perturbations asymptotically grow at the rate of, and converge to the structure of, the most unstable eigenmode. For time-dependent systems, however, the amplification at any instant may vary even though the average amplification is proscribed as $t \to \infty$, and the structure to which perturbations converge evolves in time.

3. THE UNPERTURBED SOLUTION AND THE QUASIGEOSTROPHIC MODEL

The unperturbed solution consists of an interval of 480 days taken from the statistically steady state of a damped and driven quasigeostrophic model. The characteristics of the solution as well as the quasigeostrophic equations and their numerical integration are described more fully in Snyder et al. (2001).

In this model, the flow is periodic in x and is confined between rigid surfaces at $y = 0, y_L$ and $z = 0, H$. The flow is driven by relaxation of the potential vorticity[1] (PV) to a baroclinic zonal jet and is damped by a combination of Ekman pumping at the surface and a fourth-order numerical dissipation applied to the potential vorticity. Parameters are chosen as in Snyder et al. (2001); in particular, the zonal periodicity is 16×10^3 km, the width y_L of the channel is 8×10^3 km, its depth H is 10 km, the relaxation has a time scale of 20 days, and the equilibrium zonal jet has a maximum velocity of $60\,\mathrm{m\,s^{-1}}$.

The numerical model uses a grid-point discretization. For the results shown here, there are 128 points in x, 64 in y and 8 in z.

In the statistically steady state, solutions to this model are characterized by a strong baroclinic jet in the central portion of the channel that intensifies from the surface to the lid. The flow is turbulent and exhibits an approximate power-law dependence of the velocity variance at

[1] Throughout this note, PV will refer to the generalized PV that includes contributions from the potential temperature at $z = 0, H$ in the manner of Bretherton (1966).

channel center on zonal wave number (see Fig. 3 of the following section). Meanders or waves move along the jet from east to west, with zonal wavenumbers 3 or 4 (in units of periods per channel length) dominating. These waves frequently break and form cutoff eddies in both PV and streamfunction. Snapshots of the flow are shown in Snyder et al. (2001; see also Fig. 4 here).

The structure of the PV in the statistically steady state is qualitatively similar to that of the midlatitude troposphere, as discussed for example in Hoskins et al. (1985). In particular, the horizontal PV gradient at $z = H$ is concentrated along the jet, so that the jet marks an abrupt change between regions of relatively uniform PV; the same is true to a lesser extent at the surface. Compared to those near the boundaries, however, PV gradients in the interior of the flow are small. This structure of the PV will turn out to control the structure of the leading LVs, as will be discussed in the following section.

4. STABILITY OF THE UNPERTURBED SOLUTION

a. Lyapunov exponents

Figure 1 shows estimates of the first 60 Lyapunov exponents, $\{\lambda_i,\ i = 1, \ldots, 60\}$. The leading exponent implies an (asymptotic) doubling time for perturbations of about two days. Of the remaining exponents, 35 are positive, so that the unstable subspace has dimension approximately 36, compared to the $O(10^5)$ degrees of freedom in the numerical model.

Vannitsem and Nicolis (1997), in contrast, found the unstable subspace to have dimension 102 in a different quasigeostrophic model with $O(10^3)$ degrees of freedom. The reasons for this difference are unclear, though their model has a different geometry and its flow is maintained by different forcing mechanisms.

The exponents shown in Fig. 1 should be considered estimates only, because they are based on an integration over the finite time interval $0 \leq t \leq 240$ days. The crosses in Fig. 1 indicate exponents calculated on the interval 240 days $\leq t \leq$ 480 days. The leading exponent differs by 1% between the intervals, while the second exponent differs by 8%. Although it is not central to our purpose here, the number of positive exponents is thus subject to some uncertainty.

b. Time-averaged characteristics of Lyapunov vectors

Of greater interest is the structure of the LVs and the relation of that structure to the unperturbed flow. First, consider time-averaged quantities.

The variation with height of the LV amplitude is shown in Fig. 2, in terms of both potential enstrophy (that is, the squared PV) and total energy. Values shown are the average over the first 20 LVs and over 21 times beginning at $t = 40$ days and continuing to $t = 240$ days at intervals of 10 days. (Averages over many LVs suffice because there is little variation and no systematic trend among the LVs.) The figure also displays potential enstrophy and energy for deviations of the unperturbed solution from its zonal mean.

The potential enstrophy of for the leading LVs is dominated by the top and bottom boundaries, where rms variations of the PV are a factor of 10 larger than in the interior. Consistent with the streamfunction that would be obtained by inverting such a distribution of PV, the energy is also maximized at top and bottom and decays into the interior. The unperturbed solution shares both these characteristics.

Thus, both the leading LVs and the unperturbed solution appear to be controlled by the PV at the boundaries with only a secondary contribution from the interior. Direct inversions of either the boundary or interior PV alone confirm that the flow arises mainly from the boundary PV, although the flow associated with the interior PV is not negligible. In this respect, both the leading LVs and the unperturbed solution resemble the midlatitude troposphere, where PV anomalies at the surface and tropopause are the primary dynamical agents (e.g., Hoskins et al. 1985, Davis 1992).

In the horizontal, the leading LVs possess noticeably finer scales than' the unperturbed solution. As shown in Fig. 3, the kinetic energy spectrum at $z/H = 1$ and along the channel center peaks at wavenumber 4 for the LVs instead of wavenumber 3, and has a much shallower slope in the inertial range (roughly $5 \leq k \leq 30$). This shallower slope is in accord with the predictions of closures for two-dimensional turbulence; Métais and Lesieur (1986) note that perturbations should develop a k^{-1} dependence in contrast to the k^{-3} decay of the turbulent flow.

We have also checked the dependence of the LVs on the choice of inner product by reorthogonalizing with inner products based on potential enstrophy or squared streamfunction. In fact, there is surprisingly little dependence on the inner product: we examined the first 20 LVs from 21 individual times (as in the averaging discussed above) and in all cases the projection of the ith LV for one norm onto the ith LV for another norm was greater than 0.9.

c. Instantaneous structure of Lyapunov vectors

We next consider the relation of the first LV to the instantaneous flow in the unperturbed solution. Fig. 4 shows the PV at the model top for $\mathbf{w}_1$ and the unperturbed solution at $t = 120$, 140, 160 days; these times were chosen merely as the center of the interval over which exponents and vectors were calculated.

A striking property at each of the times is the concentration of the perturbation where the unperturbed PV gradient is large. An objective measure of the relation of $\mathbf{w}_1$ to unperturbed PV gradients is the correlation of the absolute value of the perturbation PV with the magnitude of the unperturbed PV gradient. The time series of this correlation for the level $z/H = 1$, shown in Fig. 5, has a typical value of about 0.6. There is some variation in time but the concentration of $\mathbf{w}_1$ along the unperturbed PV gradient is clearly not limited to the times shown in Fig. 4.

Moreover, the perturbations are not instabilities or waves of finer scale superimposed on the unperturbed gradient: if we follow a contour of unperturbed PV, the perturbations have scales comparable or identical to the unperturbed solution. In directions parallel to the local PV gradient, however, perturbations are highly compressed. (It is this compression gives rise to the relatively flat energy spectrum of the perturbations.) Thus, $\mathbf{w}_1$ often simply represents a displacement or phase shift of features in the unperturbed solution.

In Fig. 4a, for example, $\mathbf{w}_1$ is strongly correlated with the x derivative of the unperturbed solution. Adding the perturbation to the unperturbed solution would thus shift zonally both the cutoff feature at $x = 8000$ km and, because it includes an intrusion of low PV that gives rise to a positive-negative-positive pattern of the derivative, the leading edge of the trough at $x = 6000$ km. Although the other examples shown in Fig. 4 are less clear-cut, the general principle

is clear. Snyder and Joly (1998) and Snyder (1999) give further examples of perturbations that grow as displacements or modifications of existing finite-amplitude features in an unperturbed flow.

At other levels as well, the PV of the leading LV retains its correlation with the unperturbed PV gradient. Since the unperturbed gradient has substantial vertical coherence, the perturbation PV also has slow vertical variation. This, together with the fact that by far the largest perturbation PV is found at the boundaries, insures that the streamfunction for $\mathbf{w}_1$ inherits the smooth interior structure and (typically) weak westward tilt with height of the baroclinic waves in the unperturbed solution.

Finally, all of the above characteristics are shared at least qualitatively by LVs beyond $\mathbf{w}_1$. The time-averaged correlation of the perturbation PV with the unperturbed PV gradient, for example, is between 0.5 and 0.6 for all of the first 60 LVs.

d. Singular vectors confined to a Lyapunov subspace

It is well known that, over a given finite time interval, there will be perturbations that amplify at a rate greater than λ_1. For example, as illustrated by Fig. 6, the local (in time) amplification of $\mathbf{w}_1$ may be substantially larger or smaller than that implied by λ_1. In addition, LVs other than $\mathbf{w}_1$ may have the largest amplification over a given time interval [see Fig. 4 of Vannitsem and Nicolis (1997)].

It is straightforward to calculate the perturbation within a given subspace that amplifies most over a given time interval.[3] This perturbation is the leading singular vector for the propagator

[3] Let $W(\tau)$ be the matrix whose ith column is $\mathbf{w}_i(\tau)$ for the N LVs (or indeed let those columns be any set of orthogonal unit vectors spanning a subspace of interest). Next, define $X(t) = M(\tau, t)W(\tau)$ and perform a singular value decomposition on X, so that $X = U\Sigma V^T$ where $\Sigma = \mathrm{diag}(\sigma_1, \ldots, \sigma_N)$ and U and V are orthogonal matrices. The maximum amplification is then $\sigma_1^{1/2}$ and the perturbation that achieves this is $W\mathbf{v}_1$, where $\mathbf{v}_1$ is the first column of V. In general, the columns of WV are the initial singular vectors for the interval $[\tau, t]$ constrained to the column space of W.

M constrained to the chosen initial subspace, and more generally the calculation yields a set of singular vectors that span the chosen initial subspace. Swanson et al. (2000) present a similar calculation in the context of different quasigeostrophic model.

The maximum and minimum amplification factors for the subspace spanned by the first 20 LVs are also shown in Fig. 6 for a sequence of 2-day intervals. On average, the maximum amplification is 6.1 as compared to the 2-day amplification of about 2 implied by λ_1. In addition, there is typically a perturbation that decays by about a factor of 2 over the same intervals, even though all the perturbations in the subspace grow asymptotically. For the subspaces spanned by the first 35 and first 60 LVs, the average maximum amplifications are 7.6 and 9.4, respectively, and the average minimum amplifications are 0.37 and 0.28.

The structure of the perturbation with largest amplification is, not surprisingly, qualitatively similar to that of the leading LVs. In particular, its PV is strongly correlated with the unperturbed PV gradient and it possesses scales (at least along PV contours) comparable to the unperturbed solution. The perturbation with largest amplification also typically does not resemble any single LV but has significant projection on several.

5. SUMMARY AND DISCUSSION

For the quasigeostrophic baroclinic jet considered here, the leading LVs inherit many characteristics of the unperturbed flow. In particular, like the unperturbed flow the LVs have strongest PV perturbations at the upper and lower boundaries and, consistent with this PV structure, their wind and temperature perturbations too are maximized near the boundaries and minimized in the interior. The leading LVs also have scales comparable to those of the unperturbed flow.

A key finding is that the PV perturbations associated with the leading LVs are strongly correlated with the unperturbed PV gradient. Qualitatively, these PV perturbations take the form of long strips, with scales again comparable to those of the unperturbed flow, lying along contours of unperturbed PV in regions of large PV gradients. Thus, the LVs are not instabilities or waves of smaller scale superposed on the unperturbed solution (in analogy with, say, parallel-

flow instabilities); instead, they represent displacements or modifications of existing features of the unperturbed solution.

The form of the LVs is, in retrospect, perhaps not surprising. Advection of PV controls the dynamics of the unperturbed flow and perturbations are therefore advected passively except where their velocities interact with the unperturbed PV gradient. Away from strong PV gradients, the perturbations are sheared and stretched to smaller scales by the unperturbed flow and eventually dissipated. The perturbations then, as a rough approximation, become strongly correlated at long times with the large unperturbed PV gradients at the upper and lower boundaries. This correlation is of course imperfect since the perturbation PV and the unperturbed gradients satisfy different evolution equations; for example, strong gradient need not always imply large perturbations, as the gradient may strengthen in regions where the LV has little amplitude. Snyder et al. (2001) discuss in more detail the tendency for perturbations to correlate with the unperturbed PV gradient.

Moreover, we should not expect the LVs to introduce qualitatively new structures or scales into the flow, since the LVs are in essence an instability of a turbulent flow. If the unperturbed flow were unstable to qualitatively different structures or scales, those would soon appear in the flow.

One point that we have touched upon only tangentially is the mechanism by which the LVs grow. As noted above, the simplest analogy with instabilities on parallel flow or flows with slow spatial variation, seems inappropriate. Another possibility is the notion of Farrell and Ioannou (1999) that the growth of the LVs is a consequence of the time-dependence of the unperturbed flow. It is not obvious, however, how to extend to the present case their examples, which simply make the basic state time dependent in the parallel-flow problem. A final possibility is the view put forward by Snyder and Joly (1998) and Snyder (1999), in which attention is focussed on flows with finite-amplitude structures and the potential for perturbation growth via displacements or modifications of those existing features. This view has the advantage of fitting with the phenomenology of the LVs, but we have so far been unable to develop a more complete theory

that would describe how such displacements in turn engender further perturbations of similar character.

Acknowledgments. This work began while TH was a post-doctoral fellow in the Advanced Study Program at NCAR. Both authors were also supported at NCAR in part by the US Weather Research Program.

REFERENCES

Bretherton, F. P., 1966: Critical layer instability in baroclinic flows. *Quart. J. Roy. Met. Soc.*, **92**, 325–334.

Davis, C. A., 1992: A potential vorticity diagnosis of the importance of initial structure and condensational heating in observed extratropical cyclogenesis. *Mon. Wea. Rev.*, **120**, 2409–2428.

Farrell, B. F., and P. J. Ioannou, 1999: Perturbation growth and structure in time-dependent flows. *J. Atmos. Sci.*, , **56**, 3622–3639.

Hoskins, B. J., M. E. McIntyre and A. W. Robertson, 1985: On the use and significance of insentropic potential vorticity maps. *Quart. J. Roy. Meteor. Soc.*, **111**, 877 -946.

Legras, B., and R. Vautard, 1995: A guide to Lyapunov vectors. *Proc. ECMWF Sem. on Predictability, Vol. 1*, Reading, United Kingdom, ECMWF, 143–156.

Métais, O., and M. Lesieur, 1986: Statistical predictability of decaying turbulence. *J. Atmos. Sci.*, , **43**, 857–870.

Reynolds, C. A., R. M. Errico, 1999: Convergence of singular vectors toward Lyapunov vectors. *Mon. Wea. Rev.*, , **127**, 2309–2323.

Snyder, C., and A. Joly, 1998: Development of perturbations within a growing baroclinic wave. *Quart. J. Roy. Meteor. Soc.*, , **124**, 1961–1983.

Snyder, C., 1999: Error growth in flows with finite-amplitude waves or other coherent structures. *J. Atmos. Sci.*, , **56**, 500–506.

Snyder, C., T. Hamill and S. Trier, 2001: Dynamics and statistics of forecast errors in a quasi-geostrophic model. Part I: Linear dynamics. Submitted to *J. Atmos. Sci.*, .

Swanson, K. L., R. Vautard, and C. Pires, 1998: Four-dimensional variational assimilation and predictability in a quasi-geostrophic model. *Tellus*, **50A**, 369–390.

Swanson, K. L., T. N. Palmer, R. Vautard, 2000: Observational error structures and the value of advanced assimilation techniques. *J. Atmos. Sci.*, , **57**, 1327–1340.

Toth, Z., and E. Kalnay, 1997: Ensemble forecasting at NCEP and the breeding method. *Mon. Wea. Rev.*, , **125**, 3297–3319.

Vannitsem, S., and C. Nicolis, 1997: Lyapunov vectors and error growth patterns in a T21L3 quasigeostrophic model. *J. Atmos. Sci.*, , **54**, 347–361.

FIGURE CAPTIONS

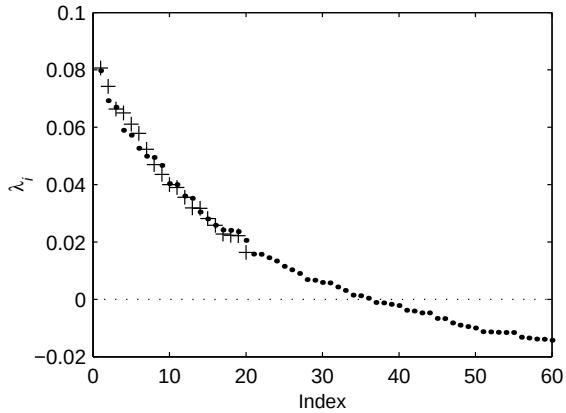

Figure 1. The first 60 Lyapunov exponents calculated over the time interval $0 \leq t \leq 240$ days (dots), and the first 20 exponents over the interval 240 days $\leq t \leq 480$ days (crosses)

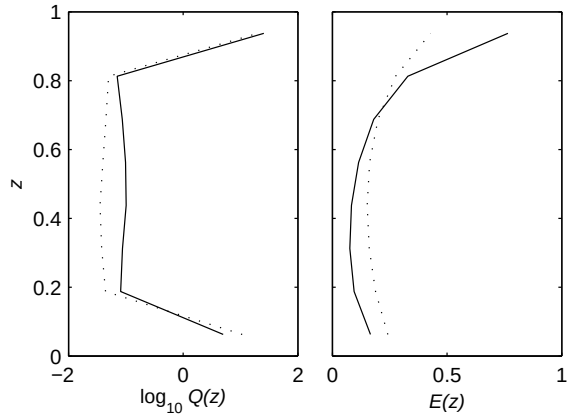

Figure 2. (a) Time- and area-averaged potential enstrophy Q as a function of height for the mean of the first 20 Lyapunov vectors (solid line) and for deviations of the unperturbed solution from its zonal mean (dotted). (b) As in (a), but for the time- and area-averaged total energy E.

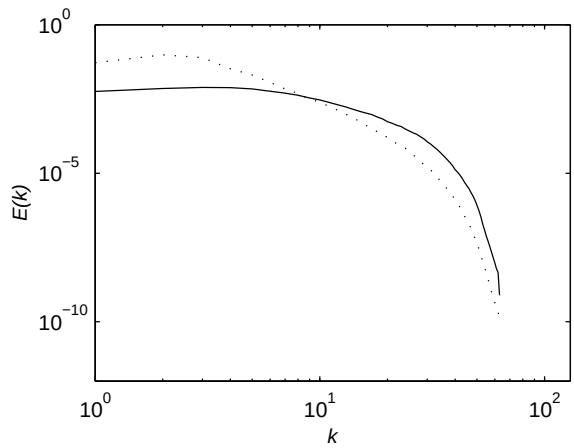

Figure 3. The time-averaged power spectra for kinetic energy at $y = y_L/2$ and $z/H = 1$. The solid line shows the mean of the first 20 Lyapunov vectors and the dotted shows the unperturbed solution.

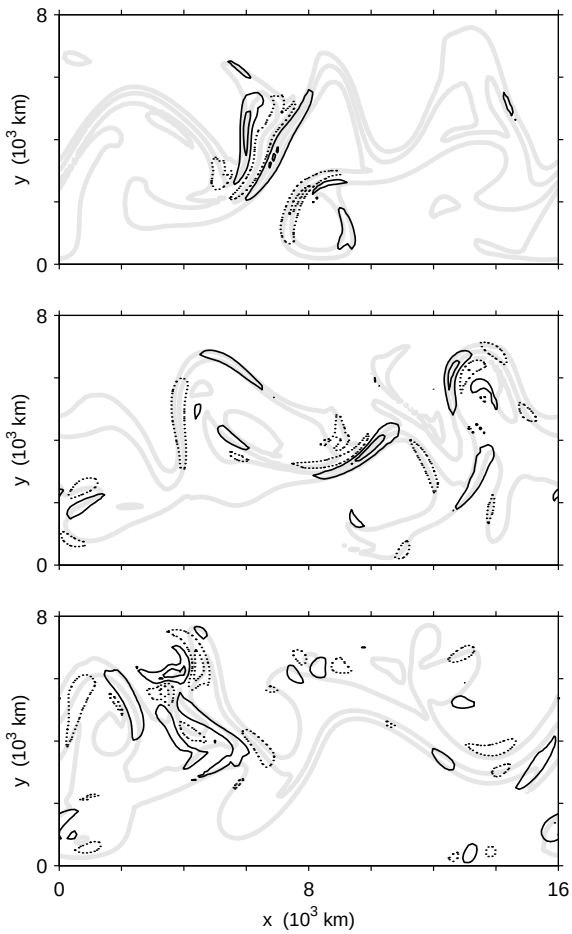

Figure 4. The PV of the leading Lyapunov vector at $z/H = 1$. Contours are shown at $1/4$ and $3/4$ of the (arbitrary) maximum amplitude and negative values dotted. Gray lines are PV contours at $z/H = 1$ for the unperturbed solution; the contour interval corresponds to about 20 K of potential temperature on the tropopause. Upper, middle and lower panels show, respectively, t = 120, 140, 160 days.

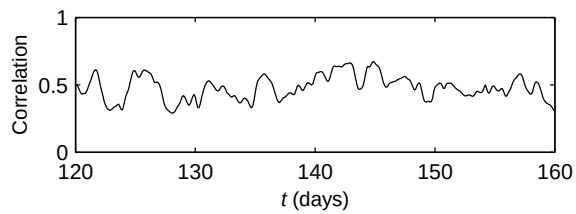

Figure 5. The correlation, as a function of time, of the square of the PV at $z/H = 1$ for the leading Lyapunov vector with the magnitude of the horizontal gradient of the unperturbed PV at the same level.

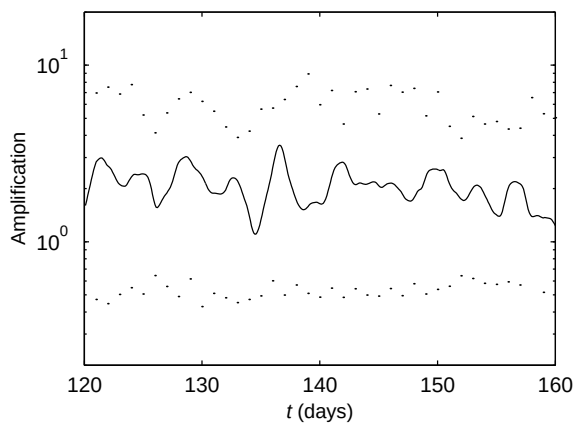

Figure 6. Two-day amplifications for the leading Lyapunov vector (solid line) and for the first and last singular vectors (dots) constrained to the subspace spanned by the leading 20 Lyapunov vectors. Amplifications are for the (square root of) total energy.